MIMO Channel Capacity Measurement in Open Square Hot Spot Access Scenarios at 300 GHz

Minghe Mao, *Member, IEEE,* Riku Takahashi, Anirban Ghosh, *Senior Member, IEEE,* and Minseok Kim, *Senior Member, IEEE*

Abstract—This letter tries to address the fundamental questions on the feasibility of multipath communication and achievable capacity for line-of-sight (LoS), obstructed-line-of-sight (OLoS), and non-line-of-sight (NLoS) scenarios in an outdoor setting for futuristic communication networks. In this context, a relevant measurement campaign at 300 GHz is conducted, and the results are presented in terms of the number of non-trivial propagation streams available for signal transmission. Encouraged by the obtained results, the average achievable channel capacity for such multi-stream channels is evaluated with and without passive reflecting surfaces (PRS). It is observed a multi-antenna system provides a significant improvement in average capacity compared to a single-antenna system with PRS providing additional enhancement.

Index Terms—Outdoor terahertz channel measurement, ultra-wideband, channel reconstruction, Ergodic channel capacity.

Fig. 1. Measurement scenario.

I. INTRODUCTION

AFTER the commercial deployment of the 5th generation (5G) mobile networks, it is now imperative to develop networks that can support higher data rates and lower latency to support envisioned futuristic applications such as metaverse, augmented reality, holographic communications to name a few [1]. To this end, the focus of the research community has shifted towards exploring frequency bands beyond 100 GHz which is expected to be the key enabler. Despite the promises of the terahertz (THz) band (> 100 GHz) due to the large stretches of bandwidth, communication in the band suffers from severe challenges due to lower output power and higher propagation loss [2]. On the other hand, an increase in transmission frequency can enable tight packing of a large number of antenna elements in a small form factor which can compensate for the additional propagation loss [3]. It is thus imperative to not only study the signal propagation in the band of interest but to also assess the potential gain of using multiple antenna systems at the transmitter (Tx) and receiver (Rx).

In this context, channel measurement and characterization have been conducted using single antenna systems at Tx and Rx for both indoor environments such as - rooms of different sizes [4], [5], corridor [6], laboratory desktop [7], data center [8] and outdoor sites such as urban environments [2], urban streets [9], and outdoor atrium [10]. Furthermore, the impact of using multiple-input-multiple-output (MIMO) systems has been investigated using the virtual antenna array concept [11], [12] in data center [13] and laboratory desktop [14], using

MIMO channel sounder in indoor setting [15], [16] and using statistical modeling for urban microcell (UMi) at 142 GHz [3]. In [16] the number of effective multiple beams in a sub-THz propagation was studied using an unidirectional sounder. The current study adds to this body of work by conducting a measurement campaign in an outdoor setting using a double-directional channel sounder to study the effectiveness of multi-stream communication at 300 GHz. To the best of the authors' knowledge, there is no precedence of the same in the literature.

This letter delineates the channel measurement campaign in an outdoor scenario using a 300 GHz channel sounder developed in-house in [5]. The data from the campaign is subsequently processed to evaluate the omnidirectional path loss (PL) synthesized by the measured power spectrum. Finally, using the single-user MIMO (SU-MIMO) evaluation methodology of [17], the ergodic channel capacity is calculated for an open square hot spot access scenario with a varying number of MIMO streams. The study explores the feasibility of using non-line-of-sight (NLoS) multipath components (MPCs) for spatial multiplexing to provide enhanced channel capacity. The effect of strategically using a passive reflecting surface (PRS) on enhancing channel capacity is also investigated.

II. MEASUREMENT CAMPAIGN

A double-directional channel measurement was conducted in an open square environment inside a university campus using an in-house 300 GHz channel sounder developed in [5]. A Newman phase multitone (NPM) signal generated by an arbitrary waveform generator (AWG) with 2560 tones and bandwidth of 8 GHz was used as the intermediate frequency

M. Mao, R. Takahashi, A. Ghosh and M. Kim are with the Graduate School of Science and Technology, Niigata University, Niigata 950-2181, Japan (e-mail: meika@eng.niigata-u.ac.jp).

A. Ghosh is also with the Department of Electronics and Communication Engineering, SRM University AP, Andhra Pradesh 522240, India.

(a) LoS: PDP at Rx03.

(b) OLoS: PDP at Rx13.

(c) NLoS: PDP at Rx15.

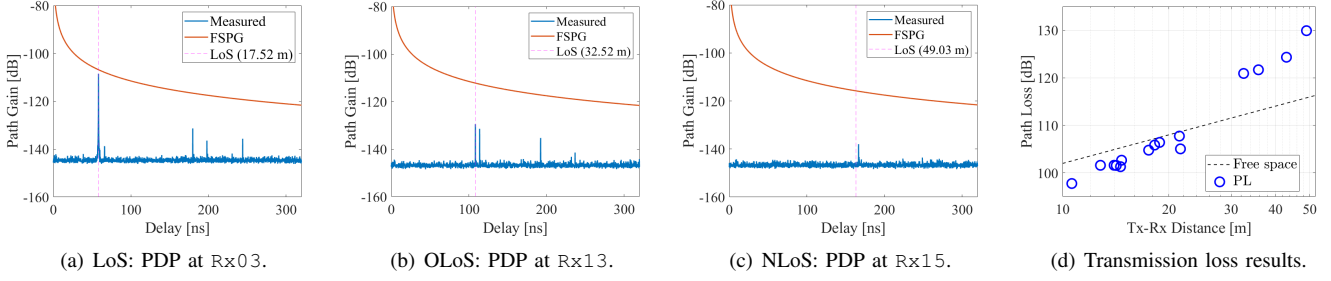(d) Transmission loss results.

Fig. 2. Channel characterization.

sounding signal during measurement producing a delay resolution of 125 ps and a maximum delay of 320 ns. The antennas at both Tx and Rx had a half-power bandwidth (HPBW) of $9°$ in the azimuth (Az) plane and a gain of 26 dBi. Due to the transmit power limit, the signal-to-noise ratio (SNR) of the received signal is expected to be adversely affected given the significant propagation loss at 300 GHz. To overcome the above-mentioned issue, the continuously received symbols were coherently averaged over 100 symbol durations during the campaign. Furthermore, back-to-back calibration was conducted before the campaign to indemnify the effect of system responses in the measured data.

During the measurement campaign, the Tx was fixed at the center of the square at a height of 3.1 m emulating an access point (AP) or a base station, and the Rx antenna was maintained at a height of 1.5 m to imitate user equipment (UE) and was moved to 15 positions within a radial range spanning 10 m $-$ 50 m. As shown in Fig. 1, the positions are labeled as Rx01-Rx15 and can be categorized into three scenarios - line of sight (LoS), obstructed LoS (OLoS) and NLoS. While Rx01 to Rx11 represent the LoS scenario, signal propagation to Rx12 and Rx13 is hindered by foliage and hence constitute the OLoS scenario. Rx14 and Rx15 fall in the NLoS category due the blockage of the LoS path by buildings in the environment. Given the difference in Tx and Rx height, the respective antennas were tilted in the elevation (El) plane by a fixed angle (θ_t) of $5°$ for proper LoS beam alignment in the absence of scanning in the same plane. The directional measurement was conducted by rotating both Tx and Rx antennas over the full azimuth angle ($0°$ to $360°$) in steps of $9°$.

III. MEASUREMENT DATA ANALYSIS

The data acquired from the measurement represent the channel transfer function (CTF), $H(\check{f}, \check{\phi}_\mathrm{T}, \check{\phi}_\mathrm{R})$, where $\check{f}$, $\check{\phi}_\mathrm{T}$, and $\check{\phi}_\mathrm{R}$ denote the samples of frequency, and azimuth pointing angles at Tx and Rx, respectively. The channel impulse response (CIR), $h(\check{\tau}, \check{\phi}_\mathrm{T}, \check{\phi}_\mathrm{R})$, is obtained by taking the inverse Fourier transform of the measured CTF, where $\check{\tau}$ denotes the delay sample. Subsequently, the double-directional angular delay power spectrum (DDADPS) is defined as the expected value of the squared absolute value of CIR as

$$P(\check{\tau}, \check{\phi}_\mathrm{T}, \check{\phi}_\mathrm{R}) \triangleq \mathbb{E}|h(\check{\tau}, \check{\phi}_\mathrm{T}, \check{\phi}_\mathrm{R})|^2, \qquad (1)$$

where $\mathbb{E}$ represents the expectation operator. Subsequently, the power delay profile (PDP) can be evaluated from the synthesized DDADPS as follows:

$$\mathrm{PDP}(\check{\tau}) = \max_{\check{\phi}_\mathrm{T}, \check{\phi}_\mathrm{R}} P(\check{\tau}, \check{\phi}_\mathrm{T}, \check{\phi}_\mathrm{R}). \qquad (2)$$

Figs. 2(a)-2(c) presents the PDP for the LoS (Rx03), OLoS (Rx13) and NLoS (Rx15) scenarios respectively. It can observed that irrespective of the scenarios, the generated PDPs are sparse and quite well separated due to the high delay resolution which can ease the process of MPC estimation and cluster identification. Furthermore, it can be noted from the results that the LoS component in Fig. 2(a) is slightly less than free space path gain (FSPG). The deviation can be attributed to the small misalignments between the Tx and Rx antennas during measurements. In comparison, the LoS component for the OLoS scenario (Fig. 2(b)) is much lower compared to FSPG due to additional loss from the obstruction by the foliage present in the path of direct signal propagation and is completely absent for NLoS (Fig. 2(c)) due to blockage by buildings.

To negate the effect of angular misalignment in the elevation plane at Tx and Rx antennas and remove the influence of noise, the previously evaluated DDADPS is further processed to generate the noise-free and misalignment-compensated DDADPS $P'(\check{\tau}, \check{\phi}_\mathrm{T}, \check{\phi}_\mathrm{R})$. The omnidirectional PL can be then calculated as follows:

$$\mathrm{PL[dB]} = -10 \log_{10} \sum_{n_\tau, n_{\phi_\mathrm{T}}, n_{\phi_\mathrm{R}}} P'(\check{\tau}, \check{\phi}_\mathrm{T}, \check{\phi}_\mathrm{R}), \qquad (3)$$

where n_τ, n_{ϕ_T} and n_{ϕ_R} are the discrete indices of $\check{\tau}$, $\check{\phi}_\mathrm{T}$ and $\check{\phi}_\mathrm{R}$, respectively. The circular markers in blue in Fig. 2(d) present the variation of the omnidirectional PL with Tx-Rx separation in comparison to free space path loss (FSPL). It can be observed from the presented results that the three investigated scenarios - LoS, OLoS, and NLoS can be distinctly identified. While the PL value is closer to the FSPL for the LoS positions (Tx-Rx separation less than 30 m), it is farther from the FSPL line in the case of OLoS and farthest for NLoS (the last two circles in blue). The results agree well with the intuition where, in the NLoS scenario the LoS paths are totally blocked compared to partial blockage in the OLoS scenario.

As the PL values in NLoS and OLoS scenarios are quite large compared to FSPL, it would be interesting to study the feasibility of communication in such scenarios for outdoor hot spot applications at 300 GHz. Furthermore, in the case of LoS

(a) Clustering at `Rx03`.

(b) Distribution of number of clusters.
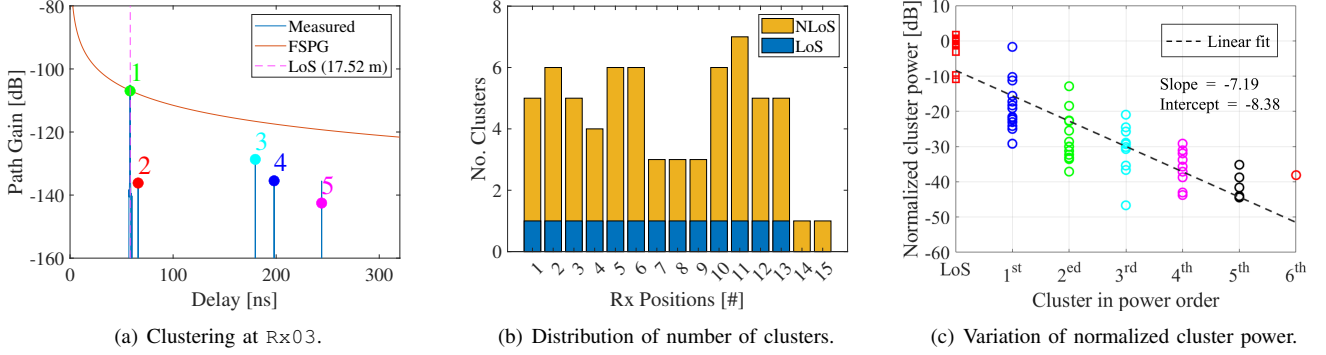

(c) Variation of normalized cluster power.

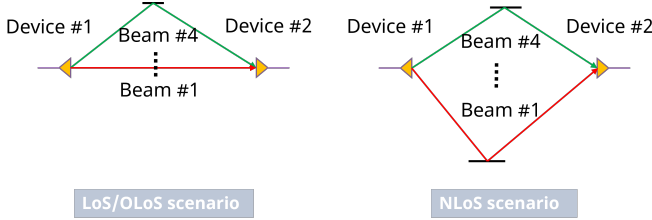Fig. 3. Clustering and its characterization.

Fig. 4. SU-MIMO transmission system model.

scenario, the number of NLoS paths and their power content relative to LoS path can provide insight into the effectiveness of using a MIMO transmission system for such outdoor access scenarios. In this context, the MPCs are extracted from the multi-dimensional, noise-free, and misalignment compensated DDADPS using the sub-grid CLEAN algorithm [18].

The algorithm assumes that the CIR consists of a group of MPCs each of which can be obtained by multiplying the autocorrelation of the sounding signal with the Tx and Rx antenna patterns. It uses a two-step peak search to estimate the delay, angular parameters, and power of the MPCs. While the first step is a coarse search over the entire measurement data, the second step comprises a finer resolution local search over a sub-grid of the measurement data to provide improved estimation. The effect of the estimated MPCs is successively removed from $P'(\check{\tau}, \check{\phi}_{\mathrm{T}}, \check{\phi}_{\mathrm{R}})$ till the algorithm converges to its preset criteria or extracts a predetermined number of MPCs. On completion, the algorithm yields a list of extracted MPCs with their estimated delays, azimuth angles of departure and arrival, and power. The estimated delay and the physical separation between Tx and Rx can be compared to easily identify the LoS and NLoS MPCs. In addition, due to the sparse nature of the PDPs as presented earlier, the extracted MPCs can be easily identified into distinct clusters.

Fig. 3(a) presents a representative result of MPC extraction and clustering at `Rx03` embedded with the synthesized PDP. The clusters are represented by colored markers and corresponding numbers. The close agreement of the LoS cluster (#1) and FSPG is to be noted. It is due to the usage of noise filtered and misalignment compensated DDADPS for MPC extraction compared to the raw DDADPS used in Fig. 2(a). Similarly, MPC extraction and clustering are done for all the

other Rx positions, and the variation in the number of extracted clusters with Rx positions is presented in Fig. 3(b). It can be observed that for the NLoS scenarios (`Rx14` and `Rx15`) there are no LoS components as expected. Additionally, for the other scenarios, the number of extracted NLoS clusters depends not only on the Tx-Rx separation but also on the scatters in the vicinity of the transceivers. The comparable number of NLoS clusters in the OLoS positions (supported by glass walls behind `Rx12` and `Rx13`) and some of the LoS positions (`Rx10` and `Rx11` surrounded by glass walls on three sides) confirm the observation. On further analysis, it is seen that on average 3.5 NLoS clusters are present. The result indicates the possibility of providing seamless connectivity through spatial multiplexing if there is sufficient power content in the NLoS clusters.

The power of the clusters normalized with FSPG for each of the Rx positions is presented in Fig. 3(c) in decreasing order. The presented plot is also fitted with a linear model having a decreasing slope of 7.19 dB. The fitted result indicates that the normalized power of the clusters differs by approximately 7 dB compared to its nearest higher-order cluster. Thus at least three to four non-trivial NLoS clusters can aid spatial multiplexing for enhanced communication.

IV. ERGODIC CAPACITY EVALUATION

A. Ergodic Capacity for SU-MIMO transmission

After exploring the feasibility of spatial multiplexing at 300 GHz, this section evaluates the ergodic capacity with multiple beams at the same frequency. In this context, the current measurement scenario is foreseen as a MIMO communication between UE and an AP in an open square. To emulate a MIMO configuration the measured angular samples (at Tx and Rx) are treated equivalently as a beam book of a phased antenna array (PAA). The illustrations of both the scenarios with or without LoS paths are shown in Fig. 4 comprising up to four streams. As the results in Section III indicate, for each position on average three to four non-trivial NLoS clusters exist hence the consideration of up to four streams in the emulation. The implemented channel model is based on the MIMO configuration of IEEE 802.11ay [17]. The Tx-Rx beam pairs are chosen depending on the power of the identified clusters. Using M Tx beams and M Rx beams, an

$M \times M$ MIMO configuration can be created. The CTF of the kth sub-carrier for the ith Rx position can be represented by $H^i(f_k, \check{\phi}_{\mathrm{T},p}, \check{\phi}_{\mathrm{R},q})$ which is a (q,p) element of the channel matrix $\mathbf{H}^{k,i}$. $\mathbf{H}^{k,i}$ can be normalized by the root mean square of the Frobenius norm as

$$\mathbf{H}_{\mathrm{norm}}^{k,i} = \mathbf{H}^{k,i}\left(\frac{1}{KM^2}\sum_{k=0}^{K-1}\|\mathbf{H}^{k,i}\|_F^2\right)^{-\frac{1}{2}}, \qquad (4)$$

$$\mathbb{E}\left[\|\mathbf{H}_{\mathrm{norm}}^{k,i}\|_F^2\right] = M^2, \qquad (5)$$

where K is the number of sub-carriers. Then, the average channel capacity for the ith Rx position is obtained as

$$C_{\mathrm{ave}}^i[\mathrm{bps/Hz}] =$$
$$\frac{1}{K}\sum_{k=0}^{K-1}\left(\log_2\det\left(\mathbf{I}_M + \frac{\rho_i}{M}\mathbf{H}_{\mathrm{norm}}^{k,i}(\mathbf{H}_{\mathrm{norm}}^{k,i})^H\right)\right), \quad (6)$$

where $\mathbf{I}_M$ is the identity matrix, $[\cdot]^H$ denotes the conjugate transpose of a matrix, and ρ_i is the single input single output (SISO) SNR of the ith Rx position. The SNR of the nearest Rx position (Rx10) with the lowest PL (approximately 10 m separation distance) is set to 30 dB [19]. For other positions, the SNR is relatively set proportional to their PL compared to the PL at Rx10.

The variation of average channel capacity with Tx-Rx separation distance for the different number of streams, M ($\in [1,2,3,4]$) is shown in Fig. 5(a), where $M = 1$ represents SISO. In addition, the solid multicolor lines in Fig. 5(c) depict the cumulative distribution function (CDF) of the average channel capacity. Generally, it is intuitive that the capacity decreases when the distance increases, and is affected severely if the LoS component is partially or completely shadowed as in OLoS and NLoS scenarios respectively. Furthermore, it is expected that the average capacity should increase with the number of streams. The results in Fig. 5(a) confirm both the intuitions where the OLoS (markers within Tx-Rx separation of 30 to 40 m) and NLoS (markers for Tx-Rx separation greater than 40 m) scenarios have the lowest capacity irrespective of the number of streams compared to any of the LoS Rx positions (markers for Tx-Rx separation less than 30 m). It is interesting to note using multi-stream propagation capacity exceeding 20 bps/Hz is achievable for an open square hot spot access scenario if the Rx is in the LoS path of Tx and is optimally placed. Even in the OLoS scenario, it is possible to support a capacity of close to 6.25 bps/Hz using a 4×4 MIMO system. Fig. 5(c) further quantifies the improvement in average channel capacity with the number of streams. It can be observed that the availability of four streams can almost double the average channel capacity compared to SISO.

As shown in Fig. 3(b), there are up to seven clusters (including LoS) when the Rx is placed in LoS path of the Tx. But on average only three to four clusters (including LoS) have significant power to be considered for multibeam transmission due to the high absorption coefficient of the materials that form the surrounding environment. It is theorized that if some PRS elements are strategically placed in the transmission environment [20], then not only the number of

non-trivial NLoS clusters will increase there might also be an improvement in the power content of the already considered NLoS clusters resulting in enhanced capacity. The feasibility study of capacity enhancement using PRS is presented next.

B. On the Feasibility of Capacity Enhancement using Reflecting Surface

Passive reflecting surfaces made of metal are assumed to be present at the interacting points of the NLoS paths to eliminate the interaction loss due to the scatterers causing the NLoS path. However, the NLoS paths are usually observed to have a gain that is slightly less than the FSPG corresponding to the path length to account for the antenna/beam pattern of the used antennas. Furthermore, as the steerable angle resolution of the equivalent multi-stream beam book as described in Section IV-A is assumed to be the same as the HPBW of the antennas ($9°$), some of the NLoS clusters with non-trivial power may be lost due to the limited angle resolution. To compensate for the interaction loss of the NLoS path, the propagation channel is reconstructed using the extracted MPCs from the measurement data. During reconstruction, power correction is introduced to negate the absorption loss effect of the scatterers due to the usage of PRS. The capacity evaluation using the reconstructed channel then follows a similar approach as described in Section IV-A.

Fig. 5(b) presents the variation of average capacity with Tx-Rx separation. It can be observed that for certain LoS positions, a capacity of up to 30 bps/Hz is achievable in a 4×4 MIMO configuration when the signal transmission is supported by the presence of PRS. The improvement is better for the OLoS positions (Tx-Rx separation between 30-40 m) where using even a 3×3 configuration can achieve a capacity of over 80 Gbps which is better than what can be achieved in a 4×4 configuration without PRS. Finally, for the NLoS scenarios (Tx-Rx separation in the range of 40 to 50 m), there is no improvement from multi-stream propagation as only one significant NLoS cluster is detected for these positions as shown in Fig. 3(b).

The improvement in average channel capacity on using PRS is presented by the multi-color dotted lines in Fig. 5(c). The usage of PRS produces an average achievable capacity which is 2.7 times greater than SISO when 4×4 MIMO channel is considered. It is to be noted that the average capacity of SISO with PRS is about 1.1 times greater than that without PRS. This is caused by the improvement in NLoS path gain of the single clusters detected at Rx14 and Rx15 as explained earlier. Thus the results indicate the efficacy of beamforming in enabling spatial multiplexing and achieving enhanced channel capacity using PRS for THz MIMO channels in outdoor hot spot access scenarios.

V. CONCLUSION

In this letter, angle-resolved three-dimensional CTFs have been acquired for three scenarios: LoS, OLoS, and NLoS using high-gain directional horn antennas in an open square at 300 GHz. The measured data is subsequently processed and the omnidirectional PL is evaluated. As expected the NLoS
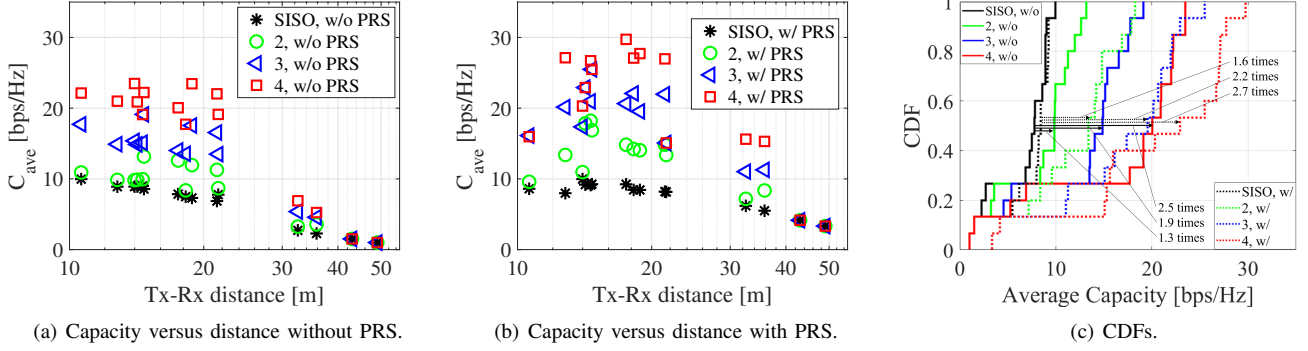
Fig. 5. Achievable channel capacity for multi-stream channels.

positions suffer from significant PL compared to FSPL followed by OLoS and LoS. To explore the feasibility of spatial multiplexing the distribution of NLoS clusters and their power content is evaluated and analyzed. It is observed an average of 3.5 NLoS clusters with non-trivial power content is present which advocates for the possibility of MIMO communication at the THz band in an open square. The advantage of using such a channel is quantified in terms of the achievable average channel capacity in the presence and absence of PRS. It is observed even without PRS an average channel capacity of more than 20 bps/Hz can be achieved in LoS scenarios if the SNR of 30 dB at 10 m separation distance can be obtained. Furthermore, for 4×4 MIMO channel when PRS is used the average channel capacity is close to three times that for SISO without PRS and a capacity of up to 30 bps/Hz is achievable.

ACKNOWLEDGMENTS

REFERENCES

[1] J. Liu, N. Kato, J. Ma and N. Kadowaki, "Device-to-Device Communication in LTE-Advanced Networks: A Survey," *IEEE Communications Surveys & Tutorials*, vol. 17, no. 4, pp. 1923-1940, Fourthquarter 2015.

[2] Y. Xing et al., "Propagation Measurements and Path Loss Models for sub-THz in Urban Microcells," in *Proc. ICC 2021 - IEEE International Conference on Communications*, Montreal, QC, Canada, 2021, pp. 1-6.

[3] S. Ju and T. S. Rappaport, "Sub-Terahertz Spatial Statistical MIMO Channel Model for Urban Microcells at 142 GHz," in *Proc. IEEE Global Communications Conference (GLOBECOM)*, Madrid, Spain, 2021, pp. 1-6.

[4] J. Gomez-Ponce et al., "Directionally Resolved Measurement and Modeling of THz Band Propagation Channels," *IEEE Open Journal of Antennas and Propagation*, vol. 3, pp. 663-686, 2022.

[5] M. Kim et al., "Indoor Channel Measurement at 300 GHz and Comparison of Signal Propagation With 60 GHz," *IEEE Access*, vol. 11, pp. 124040-124054, 2023.

[6] A. Ghosh, R. Takahashi and M. Kim, "Double-Directional Channel Characterization of an Indoor Corridor Scenario at 300 GHz," in *GLOBECOM 2023 - 2023 IEEE Global Communications Conference*, Kuala Lumpur, Malaysia, 2023, pp. 1465-1470.

[7] S. Priebe et al., "Channel and Propagation Measurements at 300 GHz," *IEEE Transactions on Antennas and Propagation*, vol. 59, no. 5, pp. 1688-1698, May 2011.

[8] C. -L. Cheng et al., "Terahertz MIMO Fading Analysis and Doppler Modeling in a Data Center Environment," in *2020 14th European Conference on Antennas and Propagation (EuCAP)*, Copenhagen, Denmark, 2020, pp. 1-5.

[9] N. A. Abbasi et al., "Double Directional Channel Measurements for THz Communications in an Urban Environment," in *2020 IEEE International Conference on Communications (ICC)*, Dublin, Ireland, 2020, pp. 1-6.

[10] Y. Li, et al., "300 GHz Channel Measurement and Characterization in the Atrium of a Building," in *17th European Conference on Antennas and Propagation (EuCAP)*, Florence, Italy, 2023, pp. 1-5.

[11] N. Maletic, L. Lopacinski, M. Goodarzi, M. Eissa, J. Gutierrez and E. Grass, "A Study of LOS MIMO for Short-Range Sub-THz Wireless Links," in *Mobile Communication - Technologies and Applications; 25th ITG-Symposium*, Osnabrueck, Germany, 2021, pp. 1-6.

[12] H. Xu, W. Wang, Y. Rui, Y. Wu, Y. Liu and L. Tang, "Virtual Antenna Array Based Wideband THz MIMO Channel Measurement," in *IEEE MTT-S International Microwave Workshop Series on Advanced Materials and Processes for RF and THz Applications (IMWS-AMP)*, Chongqing, China, 2021, pp. 222-224.

[13] C. -L. Cheng, S. Sangodoyin and A. Zajić, "Terahertz MIMO Fading Analysis and Doppler Modeling in a Data Center Environment," in *14th European Conference on Antennas and Propagation (EuCAP)*, Copenhagen, Denmark, 2020, pp. 1-5.

[14] N. Khalid and O. B. Akan, "Experimental Throughput Analysis of Low-THz MIMO Communication Channel in 5G Wireless Networks," *IEEE Wireless Communications Letters*, vol. 5, no. 6, pp. 616-619, Dec. 2016.

[15] D. Bodet, P. Dinh, M. Stojanovic, J. Widmer, D. Koutsonikolas and J. M. Jornet, "Characterizing Sub-THz MIMO Channels in Practice: a Novel Channel Sounder with Absolute Time Reference," in *2023 IEEE Global Communications Conference*, Kuala Lumpur, Malaysia, 2023, pp. 1459-1464.

[16] P. Kyösti, M. F. De Guzman, K. Haneda, N. Tervo and A. Pärssinen, "How Many Beams Does Sub-THz Channel Support?," in IEEE Antennas and Wireless Propagation Letters, vol. 21, no. 1, pp. 74-78, Jan. 2022.

[17] A. Maltsev, et al., "Channel Models for IEEE 802.11ay," *IEEE 802.11 15/1150r9*, May 2016.

[18] M. Kim, T. Iwata, S. Sasaki, J. Takada, "Millimeter-Wave Radio Channel Characterization using Multi-Dimensional Sub-Grid CLEAN Algorithm," *IEICE Trans. Commun.*, Vol.E103-B, No.7, pp.767–779, Jul. 2020.

[19] H. Tsukada, et al., "Millimeter-Wave Channel Model Parameters for Various Office Environments," *IEEE Access*, vol. 10, pp. 60387-60396, 2022.

[20] Y. Li, Y. Wang, Y. Chen, Z. Yu and C. Han, "Channel Measurement and Coverage Analysis for NIRS-Aided THz Communications in Indoor Environments," *IEEE Communications Letters*, vol. 27, no. 9, pp. 2486-2490, Sept. 2023.